Annals of Biomedical Engineering, Vol. 37, No. 5, May 2009 (© 2009) pp. 927–942
DOI: 10.1007/s10439-009-9669-2

Blood Flow in a Compliant Vessel by the Immersed Boundary Method

YONGSAM KIM,[1] SOOKKYUNG LIM,[2,4] SUBHA V. RAMAN,[3] ORLANDO P. SIMONETTI,[3] and AVNER FRIEDMAN[2]

[1]Department of Mathematics, Chung-Ang University, Dongjakgu Heukseokdong, Seoul 156-756, Korea; [2]Mathematical Biosciences Institute, Ohio State University, 231 W. 18th Ave., Columbus, OH 43210, USA; [3]244 Davis Heart & Lung Research Institute, Ohio State University, 473 West 12th Ave., Columbus, OH 43210, USA; and [4]Department of Mathematical Sciences, University of Cincinnati, 839 Old Chem, Cincinnati, OH 45221-0025, USA

(*Received 12 March 2007; accepted 3 March 2009; published online 13 March 2009*)

Abstract—In this paper we develop a computational approach to analyze hemodynamics in the aorta; this may serve as a useful tool in the development of noninvasive methods to detect early onset of diseases such as aneurysms and stenosis in major blood vessels. We introduce a mathematical model which describes the interaction of blood flow with the aortic wall; this model is based on the immersed boundary method. A two-dimensional vessel model is constructed, the velocity at the inlet is prescribed based on the information from the Magnetic Resonance Imaging data measured in the aorta of a healthy subject, and the velocity at the outlet is prescribed by driving the pressure level reproduced from the literature. The mathematical model is validated by comparing with well-known solutions of the viscous incompressible Navier–Stokes equations, i.e., Womersley flow. The hysteresis behavior in the pressure–diameter relation is observed when the viscoelastic material property of the arterial wall is taken into consideration. Five different shapes of aortic wall are considered for comparison of the flow patterns inside the aorta: one for the normal aorta, two for the dilated aorta, and two for the constrictive aorta.

Keywords—Blood flow, Immersed boundary method, Hysteresis, Aneurysm, Stenosis.

INTRODUCTION

The heart as a pump creates the pulsatile flow by alternating two phases called *systole* and *diastole*. During systole, the left ventricular pressure becomes higher than the aortic one; the aortic valve opens and the blood is pumped into the aorta. This phase occupies about one-third of the whole beat. During diastole, the ventricular pressure is balanced by the aortic pressure, the valve closes, and the ventricular pressure falls quickly, while the aortic pressure decreases slowly and the blood flows to the peripheral sites.[32,39]

Address correspondence to Sookkyung Lim, Department of Mathematical Sciences, University of Cincinnati, 839 Old Chem, Cincinnati, OH 45221-0025, USA. Electronic mail: limsk@math.uc.edu

The aortic wall consists primarily of elastin, collagen (stiffer than elastin), smooth muscle, and ground substance. The close association of elastin, collagen, and smooth muscle in the aortic wall results in viscoelastic properties that account for many of its mechanical features.[8,45] This wall expands during left ventricular systole and returns to its previous dimension during diastole. The motion of the wall is directly related to the elastic properties of the aortic wall and to the aortic pressure.[1,4,8,9,31]

Changes in elastic properties of an arterial wall and changes in the hemodynamic forces acting on it are crucial factors in potential cardiovascular diseases.[27,30,33] In this paper we present a mathematical model that describes the interaction between the arterial wall movement and the blood flow. The mathematical model is based on the immersed boundary (IB) method which was developed to study flow patterns around heart valves, and is generally a useful method for treating problems in which elastic materials interact with an incompressible viscous fluid. In the IB formulation, the fluid equations are written in Eulerian form, and the fluid variables (velocity and pressure) are stored on the fixed Cartesian coordinate system. The equations that describe the immersed boundary are written in Lagrangian form, and the boundary variables (position and Lagrangian force density) are stored on the moving curvilinear coordinate system attached to the immersed boundary. The Cartesian and curvilinear coordinates do not coincide, and the data can be transferred from one system to the other using a Dirac delta function. This method has been applied successfully to problems of blood flow in the heart,[34,35–38] wave propagation in the cochlea,[6,19] platelet aggregation during blood clotting,[14,15] animal locomotion,[10,11,13] and other biofluid problems.[3,21,23,26,29,47]

We provide a verification that the IB method correctly models and solves the interaction problem between the vessel wall and blood flow by comparing

the numerical solutions with Womersley flow in a two-dimensional straight rigid channel. Womersley flow[46] is a well-known solution for the fluid equations inside a tube when the pressure gradient is known. The pressure gradient in the longitudinal direction is changing periodically in time, while the pressure gradients in the radial and circumferential directions are zero. Since our model is two-dimensional, we consider only two components (the radial and longitudinal components).

Hysteresis is a property of physical systems that do not react immediately to the applied force. The hysteresis is observed in the relation between the blood pressure and the vessel diameter.[8] The potential parameters related to the occurrence of the hysteresis are fluid viscosity, vessel wall density, and vessel damping coefficient (viscosity of the arterial wall). We examine these factors and show that the damping coefficient is the only factor that generates the hysteresis loop in the viscoelastic arterial wall. This has been reported in literature.[1,4,9,31]

Finally, we extend the model to include cases of aneurysmal or stenotic aorta. An aneurysm is a localized bulging of blood vessels. It can occur in arteries such as the abdominal aorta, thoracic aorta, brain arteries, and coronary arteries. In contrast to an aneurysm, a stenosis is narrowing of a vessel, the most common ill-effect of atherosclerosis.[32] In the IB formulation, any deformation of the arterial wall can be constructed and its effect on the blood flow inside the artery can be analyzed. We present five different configurations and compare the flow patterns corresponding to them; these configurations are a straight but tapered artery, a symmetric dilated artery, an asymmetric dilated artery, a symmetric constrictive artery, and an asymmetric constrictive artery.

EQUATIONS OF MOTION

We begin with a mathematical formulation for a coupled system of two-dimensional viscous incompressible fluid in which an elastic boundary with mass is immersed:

$$\rho\left(\frac{\partial \mathbf{u}}{\partial t}+\mathbf{u}\cdot\nabla\mathbf{u}\right)=-\nabla p+\mu\nabla^2\mathbf{u}+\mathbf{f}, \tag{1}$$

$$\nabla\cdot\mathbf{u}=0, \tag{2}$$

$$\mathbf{F}=\mathbf{F}_{\text{ela}}+\mathbf{F}_{\text{mass}}, \tag{3}$$

$$\mathbf{F}_{\text{mass}}=-M\frac{\partial^2\mathbf{X}}{\partial t^2}, \tag{4}$$

$$\mathbf{f}(\mathbf{x},t)=\int \mathbf{F}(s,t)\delta(\mathbf{x}-\mathbf{X}(s,t))ds, \tag{5}$$

$$\begin{aligned}\frac{\partial \mathbf{X}}{\partial t}(s,t)&=\mathbf{u}(\mathbf{X}(s,t),t)\\&=\int \mathbf{u}(\mathbf{x},t)\delta(\mathbf{x}-\mathbf{X}(s,t))d\mathbf{x}.\end{aligned} \tag{6}$$

Equations (1) and (2) are the Navier–Stokes equations for a viscous incompressible fluid. The constant parameters ρ and μ are the fluid density and viscosity, respectively. The unknown functions in the fluid equations are the fluid velocity, $\mathbf{u}(\mathbf{x},t)$, the fluid pressure, $p(\mathbf{x},t)$, and the force per unit area applied by the immersed boundary to the fluid, $\mathbf{f}(\mathbf{x},t)$, where $\mathbf{x}=(x,y)$ are fixed Cartesian coordinates, and t is time.

Equations (3) and (4) are the immersed boundary equations written in Lagrangian form. The unknown $\mathbf{X}(s,t)$, the configuration of the immersed boundary at any time t, represents the arterial wall and is a one-dimensional curve in two-dimensional space. In Eq. (3), $\mathbf{F}=\mathbf{F}(s,t)$ is the force density applied by the immersed boundary to the fluid, in the sense that $\mathbf{F}(s,t)ds$ is the force acting on the fluid by a section ds of the immersed boundary. The elastic contribution $\mathbf{F}_{\text{ela}}$ to this force density is given by

$$\mathbf{F}_{\text{ela}}=c_{\text{s}}(\mathbf{Z}(s)-\mathbf{X}(s,t))-c_{\text{r}}\frac{\partial \mathbf{X}(s,t)}{\partial t}-c_{\text{b}}\frac{\partial^4\mathbf{X}(s,t)}{\partial s^4} \tag{7}$$

where c_{s}, c_{r}, and c_{b} are constants. The curve $\mathbf{Z}(s)$ represents the reference (target) configuration of the boundary which is prescribed at the beginning of computations and remains fixed in time. The first term on the right-hand side of Eq. (7) is the elastic force and its magnitude depends on the deviation of the immersed boundary $\mathbf{X}(s,t)$ from $\mathbf{Z}(s)$ and the stiffness coefficient c_{s}. The second term is the damping term which represents the viscoelastic property of the arterial wall.[9,16] The third term represents the bending resistance obtained by the variational derivative of the bending energy E_{b} as follows:

$$\lim_{\epsilon\to 0}\frac{d}{d\epsilon}E_{\text{b}}[\mathbf{X}+\epsilon\mathbf{Y}]=\int\frac{\partial E_{\text{b}}}{\partial \mathbf{X}}(s,t)\cdot\mathbf{Y}(s,t)ds, \tag{8}$$

where[7]

$$E_{\text{b}}(\mathbf{X})=\frac{c_{\text{b}}}{2}\int\left|\frac{\partial^2\mathbf{X}}{\partial s^2}\right|^2 ds, \tag{9}$$

and, according to the principle of virtual work, the bending resistance density $\mathbf{F}_{\text{b}}$ is given by

$$\mathbf{F}_{\text{b}}=-\frac{\partial E_{\text{b}}}{\partial \mathbf{X}}(s,t)=-c_{\text{b}}\frac{\partial^4\mathbf{X}(s,t)}{\partial s^4}. \tag{10}$$

The bending resistance term may have a regularizing effect when there are abrupt variations in the wall motion.

The boundary mass contribution $\mathbf{F}_{\text{mass}}$ to the force density $\mathbf{F}(s,t)$ in Eq. (3) is the inertial force (sometimes

called the D'Alembert force) written out in Eq. (4), where $M = M(s)$ is the mass density of the immersed boundary in the sense that $M(s)ds$ is the mass of a section ds of the boundary. Note that Eqs. (3), (4), and (7) are combined to yield Newton's law of motion for the immersed boundary,

$$M\frac{\partial^2 \mathbf{X}}{\partial t^2} - c_s(\mathbf{Z}(s) - \mathbf{X}(s,t)) + c_r\frac{\partial \mathbf{X}(s,t)}{\partial t} + c_b\frac{\partial^4 \mathbf{X}(s,t)}{\partial s^4} = -\mathbf{F}. \tag{11}$$

Since $\mathbf{F}ds$ is the force applied by the immersed boundary to the fluid; $-\mathbf{F}ds$ is the force applied by the fluid to the immersed boundary. Although $-\mathbf{F}$ could be expressed in terms of the jump in the fluid stress tensor across the boundary, we shall have no need to do so.

Equations (5) and (6) involve the two-dimensional Dirac delta function $\delta(\mathbf{x}) = \delta(x)\delta(y)$, which expresses the local character of the interaction between forces and velocities along the immersed boundary. Equation (5) expresses the relation between the two corresponding forces, $\mathbf{f}(\mathbf{x},t)d\mathbf{x}$ and $\mathbf{F}(s,t)ds$. We can see this by integrating each side of Eq. (5) over an arbitrary region. Note that $\mathbf{f}(\mathbf{x},t)$ has a one-dimensional delta function singularity supported on the immersed boundary. This is so because the two-dimensional Dirac delta function is a product of two one-dimensional delta functions and the integral in Eq. (5) is one-dimensional. Thus, formally, $\mathbf{f}(\mathbf{x},t)$ is infinite on the immersed boundary and zero elsewhere, but in such a manner that its integral over finite volumes is finite.

Equation (6) is the equation of motion of the immersed elastic boundary. It is the no-slip condition for a viscous fluid which states that the boundary moves at the local fluid velocity. This can also be rewritten in terms of the Dirac delta function as in the second form of Eq. (6). We do so in order to expose a certain symmetry with Eq. (5), in which the force generated by the immersed boundary is re-expressed as body force acting on the fluid. This symmetry is important in the construction of our numerical scheme. Note that the integral in Eq. (6) is a double integral $dxdy$, unlike the integral in Eq. (5) which is one-dimensional. Thus, $\partial \mathbf{X}/\partial t$ is finite, unlike $\mathbf{f}$ which has singularity of a one-dimensional Dirac delta function.

MATHEMATICAL FORMULATION OF THE PENALTY IMMERSED BOUNDARY METHOD AND NUMERICAL IMPLEMENTATION

In this section we describe how to modify Eqs. (1–6) into the penalty immersed boundary (pIB) method. The pIB method is an extension of the original IB method which assumes that the elastic boundary has no mass. The pIB method was proposed to handle the case where the mass of the immersed boundary plays an important role, for example, a flapping elastic filament in a flowing soap film.[22,24,47] The method described in this section is used to give mass to the arterial wall.

In the pIB method, we use two Lagrangian components to represent the immersed boundary. One component, denoted by $\mathbf{X}(s,t)$ and called a *massless* boundary, has no mass, is elastic, and moves at the local fluid velocity as in the original IB method. The other component, denoted by $\mathbf{Y}(s,t)$ and called a *massive* boundary, carries all the mass and is linked to $\mathbf{X}(s,t)$ by a system of stiff springs. Unlike the massless boundary, the boundary points of the massive boundary are not coupled to their adjacent points or do not interact directly with the fluid. The massive boundary moves according to Newton's law of motion in which the only force acting on such mass points is the force of the stiff springs that link the two boundaries, as shown in Fig. 1.

In mathematical terms, we obtain the pIB method by replacing Eqs. (3) and (4) by the following:

$$\mathbf{F} = \mathbf{F}_{ela} + \mathbf{F}_{pen}, \tag{12}$$

$$\mathbf{F}_{pen}(s,t) = K(\mathbf{Y}(s,t) - \mathbf{X}(s,t)), \tag{13}$$

$$M(s)\frac{\partial^2 \mathbf{Y}(s,t)}{\partial t^2} = -\mathbf{F}_{pen}(s,t). \tag{14}$$

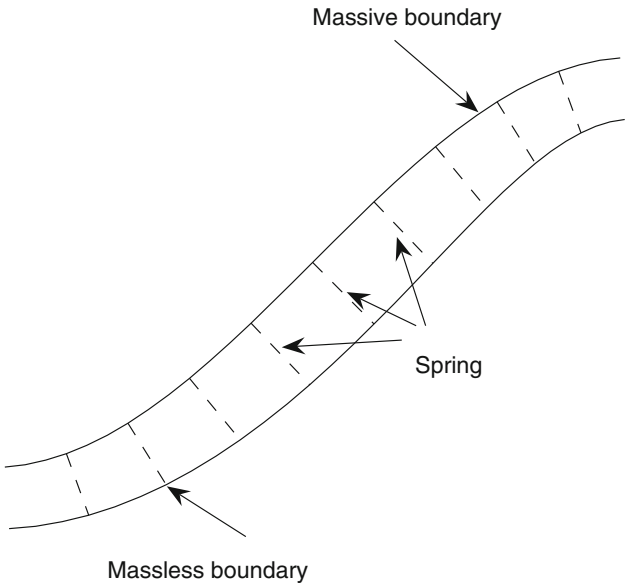

FIGURE 1. Massive and massless boundary components are linked together with a very stiff spring of which the rest length is zero.

Equation (12) defines the force density $\mathbf{F}$ transmitted by the massless boundary to the fluid. It includes the force density $\mathbf{F}_{\text{pen}}$ which is generated by the stiff springs that connect the massive and massless components of the immersed boundary, see Eq. (13). The stiffness parameter K is the *penalty* parameter of the method. The larger it is, the greater the energy penalty that must be paid to separate the two boundary components by any given amount. The limit $K \to \infty$ will be discussed below. Finally Eq. (14) is the equation of motion of the massive boundary, which carries the mass density $M(s)$ and has its motion described by the function $\mathbf{Y}(s,t)$. Note that the only force density in Eq. (14) is the penalty force density.

Consider the case in which K in Eq. (13) goes to infinity. Then the massless component $\mathbf{X}(s,t)$ and the massive component $\mathbf{Y}(s,t)$ coincide, and $\mathbf{F}_{\text{pen}}$ in Eq. (13) approaches $\mathbf{F}_{\text{mass}}$ in Eq. (4). In computations, K cannot be infinite but we can keep $\mathbf{X}(s,t)$ and $\mathbf{Y}(s,t)$ as close as we like by choosing K sufficiently large. In practice there is a stability restriction on K that depends on the time step Δt. It is empirically of the form $K\ (\Delta t)^2 < \text{constant}$. Thus, in a convergence study, the parameter K can be allowed to approach infinity as Δt approaches zero. The situation is quite favorable in that K can be multiplied by 4 every time Δt is reduced by a factor of 2. For more details of the numerical implementation of the pIB method and its convergence study, see references 22, 24.

One of the main issues in the present work is to find the crucial factors that cause hysteresis phenomena, the mass of the arterial wall being one of the candidate parameters. It turns out that the effect of this vessel mass is negligible.

What has been stated so far is the mathematical formulation of the pIB method. For its numerical implementation, we use a 'formally' second-order IB method which is described in Peskin and McQueen[38] and is generalized to take into account the massive boundary that is linked to the immersed elastic boundary by stiff springs.[22,24] In this method, each time step proceeds in two substeps, which are called the *preliminary* and *final* substeps. In the preliminary substep, we get data at time level $n+\frac{1}{2}$ from data at time level n by a first-order accurate method. Then the final substep starts again at time level n and proceeds to time level $n+1$ by a second-order accurate method. This Runge–Kutta framework allows the second-order accuracy of the final substep to be the overall accuracy of the scheme. The step-by-step procedure of the numerical implementation can be summarized as the followings:

(A) Update the position of the massless boundary at time level $n+\frac{1}{2}$. This is done by the discretization of Eq. (6). At the same time, the position of the massive boundary should evolve in the same fashion according to the velocity of the massive boundary.
(B) Using these new positions, calculate the Lagrangian force density which is the sum of two parts: one is elastic force and the other is from the spring linked between massless and massive boundaries; see Eqs. (7), (12), and (13).
(C) Change this elastic force density defined on Lagrangian grid points into the force at Eulerian spatial grid points to be applied in the Navier–Stokes equations. This is done by a discretization of Eq. (5).
(D) Given the Eulerian force density, we are ready to solve the discretized version of the fluid equations (1) and (2) at time level $n+\frac{1}{2}$. The velocity of the massive boundary is also calculated in the same fashion; see Eq. (14).
(E) Update the positions of massless and massive boundaries at time level $n+1$ in the same manner as in (A).
(F) Update the fluid velocity data by solving the fluid equation and the velocity of the massive boundary at time level $n+1$. This completes the time step.

In solving the fluid equations in both (D) and (F), we use the discrete Fourier transform (implemented by the FFT algorithm) together with the assumption of periodic boundary conditions. Note, however, that there is no fundamental requirement of using a periodic domain in conjunction with the pIB method. Any uniform grid fluid solver based on finite element or finite difference methods can be used, with whatever boundary conditions that solver can accommodate. We have emphasized the periodic case because of the efficiency that follows from the use of the FFT algorithm for solving the linear systems that arise in our numerical scheme.

TWO-DIMENSIONAL VESSEL MODEL

In this section we introduce a two-dimensional model of blood flow in a compliant vessel. We present the initial setting of our model, treatment of boundary conditions at the inlet and outlet, and physical and computational parameters used in the numerical experiments.

Consider a rectangle $[-2,2] \times [0,16]$ (cm $\times$ cm) filled with an incompressible fluid in which a compliant vessel is immersed, see the left panel of Fig. 2 which shows the initial configuration of the model. In the IB computation, the fluid exists not only inside the vessel

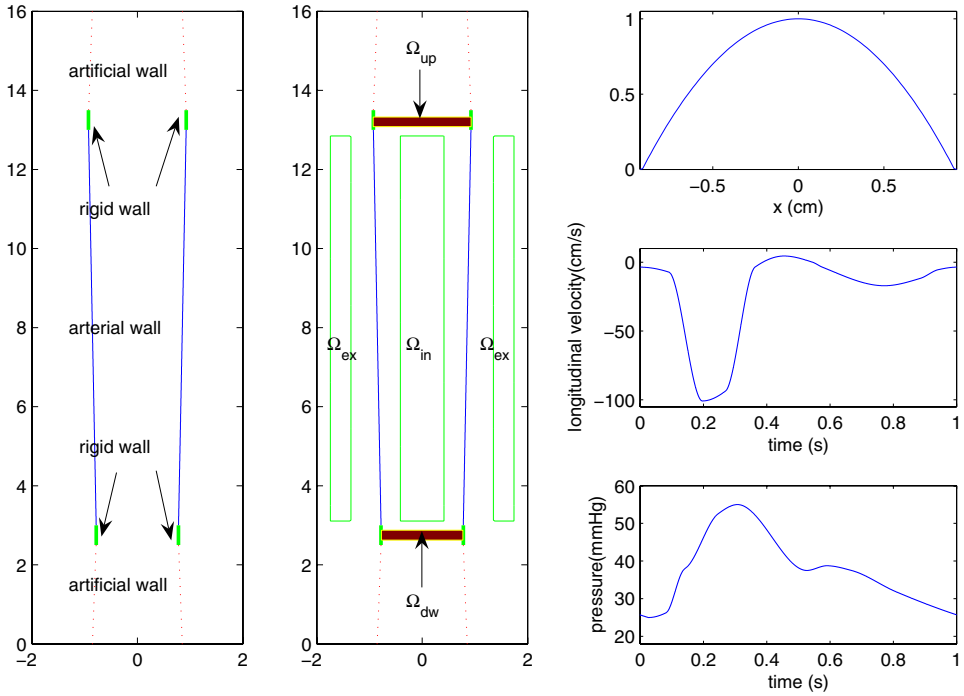

FIGURE 2. The left panel shows the initial configuration of a computational model. The two one-dimensional curves in the vertical direction are the immersed boundary in a fluid. Each curve consists of five segments: the arterial wall (solid line) in the middle, two artificial walls (dotted line) connected by two rigid bridges (thick line) to both ends of the arterial wall. The desired velocity is prescribed in the shaded regions Ω_{up} and Ω_{dw}, see the middle panel. The open rectangles Ω_{in} and Ω_{ex} inside and outside the artery are chosen to measure the pressure level, see section "Two-dimensional Vessel Model". The right-top panel shows the spatial profile of the desired velocity along the horizontal cross section of the shaded regions. The right-middle panel shows the measured velocity at the center point of the shaded region Ω_{up}, and the right-bottom panel is the desired pressure data over one cardiac cycle.

but also outside the vessel. Although the outside of the vessel is occupied by tissues or other organs, we assume that the fluid is everywhere.

In the computational domain there are two separate immersed boundaries (two one-dimensional curves in the longitudinal direction) which represent the wall of the aorta, and each boundary curve is composed of five parts: one arterial wall (solid line) in the middle, two artificial walls (dotted line) at the top and bottom, and two rigid bridges (thick line) connecting the arterial wall and the artificial wall; see the left panel of Fig. 2. Note that we focus on the motion of the arterial wall (solid line) which is symmetric and tapered. The artery has the radius R_{up} at the upstream section and the radius R_{dw} ($< R_{up}$) at the downstream section. The region surrounded by the artificial wall works as a reservoir. The pulsatile motion of the arterial wall, which is induced by the inflow and the outflow of the artery, can change the volume of the region surrounded by the arterial wall. This volume change is compensated by the opposite change of the volume of the region surrounded by the artificial wall. Note that the rigid bridge which connects the arterial wall to the artificial wall is also a part of the immersed boundary.

The reference configuration represented by $\mathbf{Z}(s)$ in Eq. (7) is the target position of the immersed boundary and is chosen as an initial configuration. The immersed boundary $\mathbf{X}(s,t)$ in Eq. (7) moves in time close to the reference position $\mathbf{Z}(s)$. How much $\mathbf{X}(s,t)$ can deviate from $\mathbf{Z}(s)$ depends inversely on the stiffness coefficient c_s in Eq. (7). For a normal vessel we consider a tapered and straight boundary as a reference configuration of the arterial wall (solid line); see Fig. 2. We shall later change the reference configuration into a curve to take into account bulging and constrictive arterial walls.

The two shaded regions Ω_{up} and Ω_{dw} inside the rigid bridges in the middle panel of Fig. 2 are used to prescribe the *desired* velocity in the following way. Let Ω_0 be the union of the two shaded regions; one region at the top is denoted by Ω_{up} and the other region at the bottom is denoted by Ω_{dw}. The way of driving a flow in Ω_0 is to apply an external force per unit area equal to

$$\mathbf{f}_0(\mathbf{x},t) = \begin{cases} \alpha(\mathbf{u}_0(\mathbf{x},t) - \mathbf{u}(\mathbf{x},t)), & \mathbf{x} \in \Omega_0 = \Omega_{up} \cup \Omega_{dw} \\ 0, & \text{otherwise}, \end{cases} \tag{15}$$

where $\mathbf{u}_0(\mathbf{x},t) = (u_0(\mathbf{x},t), v_0(\mathbf{x},t))$ is the desired velocity with the radial and longitudinal components and α is a

constant. This force will be added to the right-hand side of Eq. (1). When α is large, the fluid velocity $\mathbf{u}$ is driven rapidly towards $\mathbf{u}_0$ within Ω_0.

The radial component $u_0(\mathbf{x},t)$ of the velocity $\mathbf{u}_0(\mathbf{x},t)$ is actually very small and is therefore assumed to be zero in both Ω_{up} and Ω_{dw}. This implies that there is no transversal flow in the inlet and outlet. The longitudinal velocity $v_0(\mathbf{x},t)$ in Ω_{up} (Ω_{dw}) is defined by

$$v_0(\mathbf{x},t) = v_{center}(t) \times g(\mathbf{x}) \tag{16}$$

where $\mathbf{x}$ is the fixed Cartesian coordinates of the horizontal cross section in Ω_{up} (Ω_{dw}), $v_{center}(t)$ is the velocity at the center of that cross section, which usually reaches the maximum magnitude of the longitudinal velocity at the upstream (downstream), and $g(\mathbf{x})$ is the spatial profile along the horizontal cross section of Ω_{up} (Ω_{dw}) which is parabolic; see the right-top panel of Fig. 2. The time-dependent velocity $v_{center}(t)$ in Ω_{up} is the measured MR data over a cardiac cycle (right-middle panel of Fig. 2), while the velocity $v_{center}(t)$ in Ω_{dw} is the computed value which will be described below to satisfy the pressure condition (right-bottom panel of Fig. 2).

A human aorta is a shape of a Christmas candy cane, and the scanned cross sections are where the aorta runs approximately straight. Velocity and radius are measured at the two cross sections which are spaced at 10 cm apart; see Fig. 3. The MRI scan was performed in the aorta of one of the authors at the hospital at Ohio State University. The methodological detail of the MR data acquisition technique is as follows: velocity-encoded imaging was obtained using a retrospectively electrocardiographically gated, breath-hold gradient-echo, phase-contrast sequence with a velocity sensitivity of 150 cm/s prescribed at proximal and distal cross-sections of a relatively straight segment of the descending thoracic aorta. The following scan parameters were typically used: matrix 132 × 192 pixels, field of view 275 × 400 mm, slice thickness 6 mm, bandwidth 355 kHz/pixel, temporal resolution based on heart rate, TE 2.0 ms, and flip angle 25°.

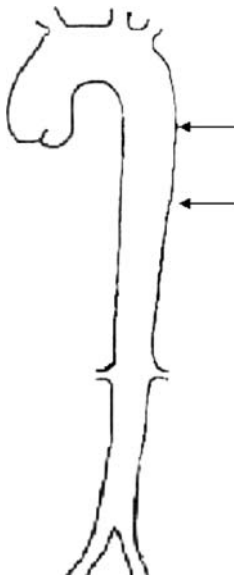

FIGURE 3. A human aorta. Redrawn after Boudoulas *et al.*[8] We model the region between the two arrows where the MR data (velocity and radius) are measured.

Now we describe the method to compute the velocity at the center in Ω_{dw}. Whereas the velocity at the center in Ω_{up} comes from the MR data, the velocity at the center in Ω_{dw} is computed so that the pressure across the wall of the blood vessel matches the *desired* pressure reproduced from Nichols and O'Rourke[32] as shown in the right-bottom panel of Fig. 2. The desired pressure data is chosen to be around 50% of the data of Nichols and O'Rourke[32] in order to avoid numerical instabilities. The way of computing the axial velocity $v_0(\mathbf{x},t)$ in Ω_{dw} is the following: choose an interior region of the artery Ω_{in} and exterior regions of the artery Ω_{ex}, see the open rectangles inside and outside the artery in the middle panel of Fig. 2. Then the average pressure p_{in} in Ω_{in} can be computed by

$$p_{in} = \frac{1}{\text{Area}(\Omega_{in})} \int_{\Omega_{in}} p(\mathbf{x},t)d\mathbf{x}, \tag{17}$$

where $p(\mathbf{x},t)$ is the fluid pressure and $\text{Area}(\Omega_{in})$ represents the area of Ω_{in}. The average pressure p_{ex} in the external region Ω_{ex} is defined in the same fashion.

Just as the real blood pressure is the pressure inside the artery relative to the reference atmospheric pressure, so we use the pressure p_{ex} as a reference pressure and define the computational pressure level as $p_{in} - p_{ex}$. It is desirable to keep $p_{in} - p_{ex}$ close to the measured blood pressure. In order to enforce this condition, we use the following feedback mechanism:

$$(Q_{up} - Q_{dw}) = \beta(\tilde{p}(t) - (p_{in} - p_{ex})), \tag{18}$$

where $\tilde{p}(t)$ is the *desired* blood pressure and β is a positive constant. The quantities Q_{up} and Q_{dw} are the flow rates (fluxes) of blood coming in Ω_{up} and leaving out Ω_{dw}, respectively. The flow rate Q_{up} is obtained by integrating the desired velocity from the MR data over a horizontal line in the region Ω_{up}. Since the blood pressure level $\tilde{p}(t)$ is also given and the pressure difference $(p_{in} - p_{ex})$ can be computed in each time iteration, we can get Q_{dw} using the relation (18). With this computed flux Q_{dw} and the given spacial profile $g(\mathbf{x})$ in Ω_{dw}, we can obtain the longitudinal velocity at the center in Ω_{dw} which is then used to construct the desired velocity $v_0(\mathbf{x},t)$ in Ω_{dw}.

Note that $(Q_{up} - Q_{dw})$ represents the rate of change of the blood volume inside the artery. Equation (18)

implies that, when the computational blood pressure $(p_{in} - p_{ex})$ is lower than the target pressure $\tilde{p}$, the value Q_{dw} decreases so that more blood flows in than flows out. This results in increased volume of the artery and increased pressure. On the contrary, the computational pressure $(p_{in} - p_{ex})$ larger than the desired pressure $\tilde{p}$ leads to the increase of Q_{dw} and the decrease of both the internal blood volume and the pressure. This feedback mechanism allows us to keep the computed pressure level close to the target blood pressure.

Table 1 lists physical and computational parameters. The fluid density and viscosity are those of the typical blood in major arteries. The dimensions of the vessel such as arterial radius and length are chosen from the MR data. Note that the artery has a larger radius at the upstream than at the downstream. The arterial wall density M and stiffness coefficient c_s are close to the value observed in literature.[8,9,16,32] In references 9, 16, the authors calculated the stiffness coefficient c_s by the following formula:

$$c_s = \frac{E_Y h}{(1-\sigma^2)R^2}\,(\mathrm{dyn/cm^2}), \tag{19}$$

where E_Y is Young's modulus of elasticity and σ is the Poisson ratio, h is the wall thickness, and R is the radius of the vessel. Canic *et al.*[9] used the values from 9.3×10^4 to 7.4×10^6 (dyn/cm^2) and Formaggia *et al.*[16] used 6×10^5 (dyn/cm^2). The bending coefficient c_b is chosen to guarantee that an undesirable saw-toothed motion of the wall is removed. It is natural to observe a shape of the tiny saw-toothed wall without bending resistance, and this undesirable shape eventually leads to computational instability. We prevent from the saw-toothed motion of the wall by adding a small bending resistance. We observed, however, that when the bending coefficient c_b varied from 20 dyn/cm^2 to about 100 dyn/cm^2, the overall motion of the wall with different bending resistances was almost the same. This is so because the force from the stiffness of the wall dominates other forces including the bending resistance. The damping coefficient c_r representing the viscoelastic property of the arterial wall varies and is an important parameter which, in our simulation, enables the blood flow in the compliant artery to have the hysteresis phenomena. The high dependence of the hysteresis on the viscoelastic material property was claimed by Canic *et al.*[9] For comparison of the values for viscoelastic coefficient, Canic *et al.*[9] derived the viscous modulus c_r to be 1.6×10^4 (dyn s/cm^2) for the human femoral artery. This value is of the same order of magnitude as the measurements corresponding to the dogs aorta reported in Armentano *et al.*[1,2] For numerical simulations, they used larger values for aorta ranging from 1×10^4 to 8×10^4 (dyn s/cm^2).

TABLE 1. Physical parameters.

Parameters	Magnitude
Fluid density, ρ	1.05 g/cm^3
Viscosity, μ	0.04 g/(cm s)
Arterial wall density, M	1.06 g/cm^3
Arterial length	10.0 cm
Arterial radius, R_{up}	0.925 cm
Arterial radius, R_{dw}	0.78 cm
Stiffness coefficient, c_s	7×10^5 dyn/cm^2
Bending coefficient, c_b	40 dyn cm^2
Artery damping, c_r	0–8000 (dyn s/cm^2)
Computational domain	4×16 cm^2
Computational grid size	256×1024

Once we have constructed the initial configuration of the vessel model and set the physical parameters, we solve Eqs. (1)–(2), (5)–(7), and (12)–(14) using the numerical procedure described in section "Mathematical Formulation of the Penalty Immersed Boundary Method and Numerical Implementation". The mesh-width of the computational domain is taken to be $\Delta x = \Delta y = 4/256$ (uniform and fixed in time), and the time duration is taken to be $\Delta t = 5 \times 10^{-6}$ s.

VALIDATION OF THE MATHEMATICAL MODEL

In this section we validate the robustness of our mathematical model by comparing the results with a well-known analytical solution of the Navier–Stokes equations. Womersley flow[46] is a solution of the fluid equations in a cylindrical pipe when the pressure gradient is periodic. Since we consider a fluid in a 2D straight rigid channel instead of a cylindrical pipe, we first derive the exact form of the analytical solution which is slightly different from the original Womersley flow.

Given equations for an incompressible viscous fluid in 2D:

$$\rho\left(\frac{\partial \mathbf{u}}{\partial t} + \mathbf{u}\cdot\nabla\mathbf{u}\right) = -\nabla p + \mu\nabla^2\mathbf{u}, \tag{20}$$

$$\nabla\cdot\mathbf{u} = 0. \tag{21}$$

The pressure gradient is also given: $\frac{\partial p}{\partial y} = Ae^{i\omega t}$ (y-directional pressure gradient); $\frac{\partial p}{\partial x} = 0$ (x-directional pressure gradient). Since there is no flow in the x direction, i.e., $u = 0$, the fluid equations can be reduced to $\rho v_t + Ae^{i\omega t} = \mu v_{xx}$. Letting $v = Ve^{i\omega t}$, we then obtain $i\omega\rho V + A = \mu V_{xx}$. Now let $x = Rz$ and $\tilde{V}(z,y) = V(x,y)$ where R is the radius of the 2D channel and $-1 \le z \le 1$. Then $\tilde{V}_{zz} - i\alpha^2\tilde{V} = \frac{AR^2}{\mu}$ where $\alpha = R\sqrt{\rho\omega/\mu}$ is Womersley number. The solution of

the latter equation with the boundary conditions $\tilde{V}(\pm 1, y) = 0$ is given by

$$\tilde{V} = \frac{iAR^2}{\mu\alpha^2}\left(1 - \left(e^{\alpha\sqrt{i}} + e^{-\alpha\sqrt{i}}\right)^{-1}\left(e^{\alpha\sqrt{i}z} + e^{-\alpha\sqrt{i}z}\right)\right). \tag{22}$$

Thus the longitudinal velocity in 2D Womersley flow is

$$\begin{aligned} v(x,y,t) &= \frac{iAR^2}{\mu\alpha^2}\left(1 - \left(e^{\alpha\sqrt{i}z} + e^{-\alpha\sqrt{i}z}\right)\Big/\left(e^{\alpha\sqrt{i}} + e^{-\alpha\sqrt{i}}\right)\right)e^{i\omega t} \\ &= \frac{iA}{\rho\omega}\left(1 - \left(e^{\alpha\sqrt{i}x/R} + e^{-\alpha\sqrt{i}x/R}\right)\Big/\left(e^{\alpha\sqrt{i}} + e^{-\alpha\sqrt{i}}\right)\right)e^{i\omega t}. \end{aligned} \tag{23}$$

If we were to take the real part of the longitudinal pressure gradient $Ae^{i\omega t}$, the corresponding flow would be the real part of Eq. (23).

Now we shall drive Womersley flow numerically by our model, and compare its result with the exact solution given in Eq. (23). To do that, we choose the two radii of the artery, R_{up} and R_{dw}, to be the same $R = 0.925$ cm so that the artery becomes a 2D channel immersed in a fluid, and set the coefficient c_s in Eq. (7) to be very large. Note that a large coefficient c_s prevents the arterial wall from moving, so that the arterial wall can be considered as a fixed boundary. In order to generate Womersley flow in the channel we use two different approaches: one approach is to apply sinusoidal force as an external force in the right-hand side of Eq. (1), and the other approach is to prescribe the exact solution of Womersley flow only in the shaded regions (Fig. 2) in the way described in section "Two-dimensional Vessel Model"; see Eq. (15).

In the first approach, we apply an external sinusoidal force $A\cos(\omega t)\mathbf{e}_2$ to the fluid equation (momentum equation), where $\mathbf{e}_2$ is the unit vector in the upward direction. We use $\omega = 2\pi$ which makes the Womersley number $R\sqrt{\rho\omega/\mu}$ be around 4.7. Since the applied sinusoidal force acts as a pressure gradient inside the channel, it should generate Womersley flow. Note, however, that the body force is applied to the whole domain as well as to the inside of the channel. The left panel of Fig. 4 shows the longitudinal velocity $v(\mathbf{x},t)$ at different times. These times are chosen in the 4th cycle in order to remove the effect of initial values. The left panel in Fig. 4 shows excellent match of our simulation of Womersley flow to the exact solution. Moreover, even though we apply the sinusoidal force to the whole domain, the flow inside the channel is almost the same as Womersley flow. This result also shows that the fixed channel created by a large coefficient c_s in Eq. (7) prevents the flow outside the channel from affecting the dynamics inside the channel.

In the second approach, we apply the body force of the form in Eq. (15) to the fluid equation in which Ω_0 is the shaded regions in Fig. 2 and the desired velocity $v_0(\mathbf{x},t)$ is the solution of Womersley flow. That is, the inlet and outlet boundary conditions of the vessel are time-dependent solution of Womersley flow. Since the fluid equations (1) and (2) with given initial and boundary conditions have a unique solution, and the flow at the inlet and outlet of the channel are given as Womersley flow, the fluid equations should result in Womersley flow in the whole channel. The right panel of Fig. 4 compares the numerical results with the exact solutions of Womersley flow at different times. Here again, the exact solution and the numerical solution

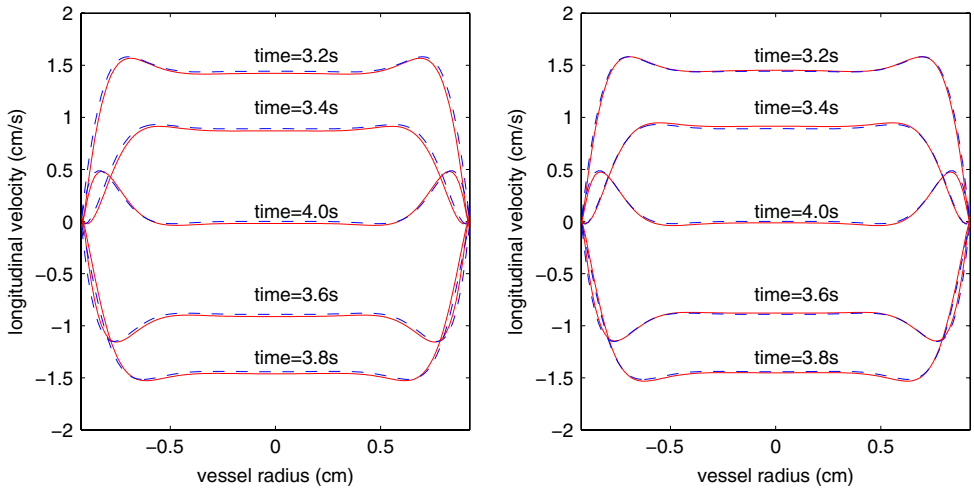

FIGURE 4. A comparison of the numerical solutions (solid line) with Womersley solutions (dashed line) at different times. *Left*: The sinusoidal force is applied to the whole fluid domain. *Right*: The exact solution of Womersley flow is chosen as a desired velocity in the inlet and outlet of the vessel, see Eq. (15). The Womersley number $R\sqrt{\rho\omega/\mu}$ is around 4.7.

almost coincide. Note that, since Womersley flow is generated inside a pipe of which the boundary is fixed without moving, it is not necessary to consider a larger computational domain than the cylindrical pipe. However, in order to consider a moving compliant vessel, we need more space for the channel boundary to be able to move, and our method can handle this case too, as will be shown in the next section.

RESULTS

We first discuss the method to achieve desired flows in both Ω_{up} and Ω_{dw}. The method described in section "Two-dimensional Vessel Model" is to add Eq. (15) as an external body force term on the right hand side of the Navier–Stokes (momentum) equation. When α in Eq. (15) is large, the velocity at the fixed Cartesian coordinate is driven rapidly towards $\mathbf{u}_0(\mathbf{x},t)$ within Ω_{up} (Ω_{dw}). In particular, the approach of $\mathbf{u}(\mathbf{x},t)$ to $\mathbf{u}_0(\mathbf{x},t)$ within Ω_{up} (Ω_{dw}) will occur approximately exponentially with a time constant equal to ρ/α. Thus, in order for the Navier–Stokes equations to produce inflow/outflow velocity close to the desired inflow/outflow, the constant α should be large enough, but not too large, for a very large α can be a source of numerical instability. We can resolve this dichotomy by reducing the time step Δt.

Figure 5 shows the velocities at the center in the upper region Ω_{up} (left) and the lower region Ω_{dw} (right). The dashed lines represent the desired velocities in time and the solid lines represent the computed velocities in time. The computed velocity is at most 15% off the desired velocity during systole. We consider these computational results quite satisfactory, and we shall therefore rely on the boundary conditions in the inlet and outlet regions which were used to derive the numerical results of Fig. 5.

The interior pressure of the artery relative to the exterior pressure of the artery follows the compliance relation which says that the relative pressure depends proportionally on the volume of the blood inside the artery. We control the outflow in Ω_{dw} and, thus, the volume inside the artery, in order to keep the computed pressure close to the target pressure data; see Eq. (18). Just like α in Eq. (15), the computed pressure can be driven rapidly towards the pressure data by choosing the constant β large enough. We chose a moderate value of β in order not to introduce a numerical instability.

The left panel of Fig. 6 illustrates the change of the blood pressure in time: the dashed line represents the desired pressure and the solid line represents the computed pressure. The latter reaches 82% of the former at the systolic phase. The right panel of Fig. 6 shows the diameter of the artery as a function of time calculated at the center of the artery over two cardiac cycles. Time is chosen after one cardiac cycle in order to remove the transient time. The diameter changes by about 5.2% from its diastolic minimum to its systolic maximum, which is similar to the MR and other data.[32] The patterns in the two panels look very similar and indicate pulsatile dynamics.

Even though in real arteries the pressure inside the artery and the diameter of the artery have the same qualitative behavior as in Fig. 6, their detailed behavior is different. The arterial wall does not instantly follow the pressure applied to the wall, but it reacts slowly, and *hysteresis* occurs. In order to detect the hysteresis, we varied some parameters of our model and investigated the relationship between the pressure and the diameter. The variable parameters were the arterial mass density M, the fluid viscosity μ, and a damping coefficient c_r that represents the viscoelastic property of the arterial wall. When the wall density ranged from 0.106 to 106.0 (g/cm^3), or when fluid viscosity varied from 0.004 to 4.0 (g/cm s), we did not observe the hysteresis. However, hysteresis appeared when the damping coefficient was changed.

Figure 7 shows the relationship between the pressure (x-axis) and the wall diameter (y-axis) with

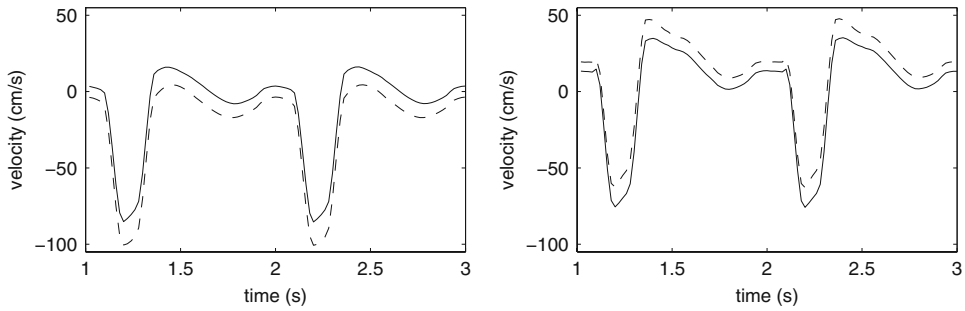

FIGURE 5. A comparison of the measured velocity and the computed velocity over two cardiac cycles in the lower region Ω_{dw} (left) and the upper region Ω_{up} (right). The velocities are taken at the center of the regions Ω_{dw} and Ω_{up}. The computed velocity (solid line) stays close to the measured velocity (dash-dot line) in both regions.

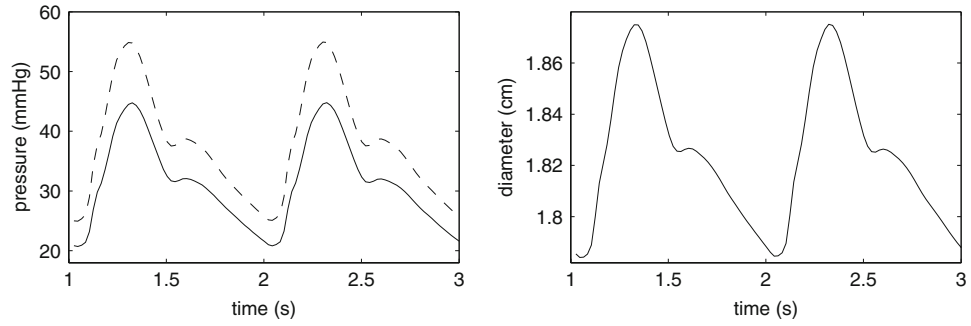

FIGURE 6. The left panel shows the blood pressure as a function of time: the dashed line represents the desired pressure and the solid line represents the computed pressure. The right panel shows the diameter of the artery over two cardiac cycles which is measured at the center of the vessel. The two figures indicate the pulsatile dynamics of the arterial vessel. The diameter changes by about 5.2% from its diastolic minimum to its systolic maximum.

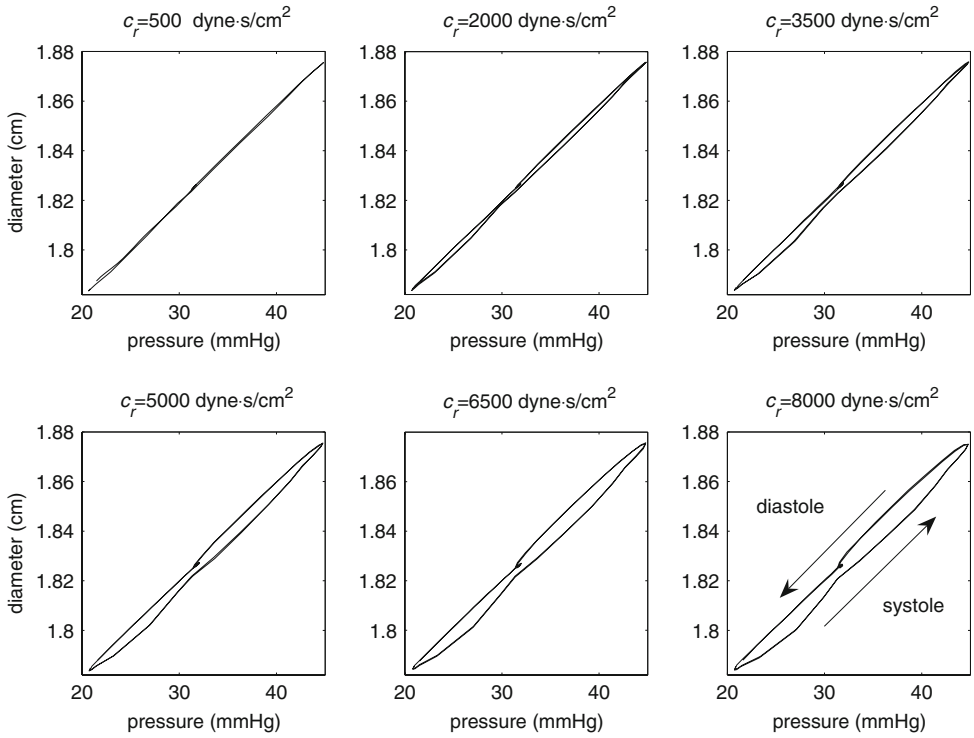

FIGURE 7. Relationship between the pressure (*x*-axis) and the wall diameter (*y*-axis) with the six different damping coefficients. The hysteresis loop appears clearly as the damping parameter c_r increases. The loop turns in counterclockwise direction in time.

different damping coefficients. When the damping coefficient c_r is small up to 500 (dyn s/cm^2), the arterial wall responds immediately to the pressure, and thus the relation between the diameter and the pressure is almost linear. As this damping coefficient increases, however, this relation becomes nonlinear, and a hysteresis loop appears. In the hysteresis loop the change of the pressure precedes that of the diameter. The amount of time delay in the motion of the artery compared to the pressure change depends proportionally on the magnitude of the damping coefficient; compare the size of the closed regions in the figure. Note that the loops in the figure are drawn in the counterclockwise direction in time.

We now extend our model to simulate and study the blood flow in aneurysmal or stenotic arteries. Aneurysm is a dilatation of a blood vessel; a portion of the arterial wall weakens and bulges outward. Stenosis is a narrowing of a blood vessel. The most common ill-effect of atherosclerosis is stenosis, resulting in a reduction in blood flow to the tissues. The exact pathogenesis of these diseases is not known. However, studies suggest that the cause of the diseases is the interaction between the changes in the hemodynamics

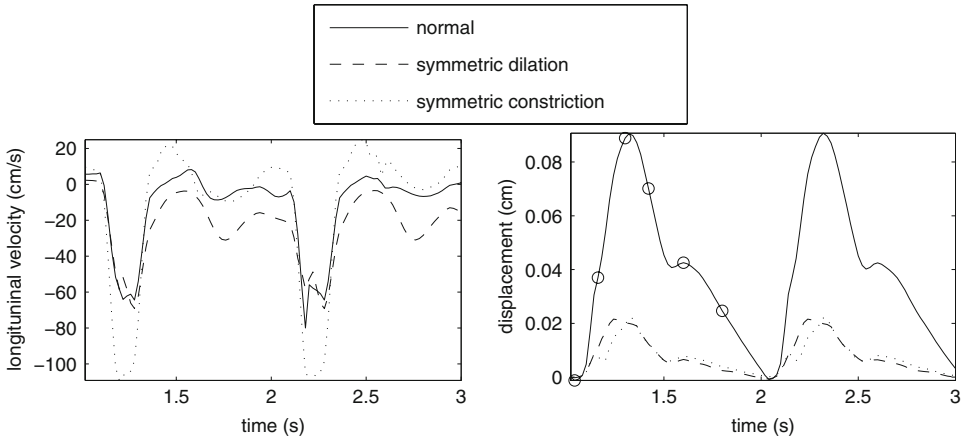

FIGURE 8. Comparison of the longitudinal velocity (left panel) and the radial displacement of the vessel wall (right panel) with three different shapes: normal (solid line), symmetric dilated (dashed line), and symmetric constrictive arteries (dotted line). The radial displacement is measured at the middle cross section of the vessel, and the longitudinal velocity is taken at the mid-point of that cross section during two cardiac cycles. The six circles '○' in the right panel indicate the times chosen for Figs. 9–13.

on the arterial wall and the biological processes in the blood vessel.[5,8,12,17,18,20,25,27,28,32,41,42,44]

Since the IB method for the fluid–structure interaction can handle almost arbitrary shape of the immersed structure regardless of its flexibility, we can construct the configuration of a vessel related to a pathological deformation and use the IB method to investigate the blood–vessel interaction. Here, we take into account arterial walls in five different shapes: normal, symmetric dilated, asymmetric dilated, symmetric constrictive, and asymmetric constrictive (see Figs. 9–13). The dilated or constrictive height in the radial direction is 0.35 cm (41% of the normal vessel radius) for both symmetric and asymmetric cases. For all these simulations, we use the same data (velocity and pressure) and the physical and computational parameters as used earlier in the normal case.

Figure 8 illustrates the comparison of the longitudinal velocity (left panel) and the radial displacement of the vessel wall (right panel) with three different shapes: normal (solid line), symmetric dilated (dashed line), and symmetric constrictive (dotted line) arteries. The radial displacement is measured at the middle cross section of the vessel, and the longitudinal velocity is taken at the mid-point of that cross section. Whereas the flow speed in the bulging artery is close to that of the normal artery in systolic phase, the flow speed in the stenotic artery is much faster in systole and varies more than those in the former two cases. This means that the blood moves faster as an artery gets narrower. The qualitative behaviors of the wall movement in the three cases are almost the same, see the right panel of Fig. 8. However, the displacement of the artery in the normal case is larger than those in the abnormal cases. This is because we chose a smaller β in Eq. (18) for the abnormal cases in order to avoid a numerical instability.

Figures 9–11 show vorticity contours (top) and pressure contours (bottom) in the three different shapes of arteries at some fixed times. Vorticity is related to the amount of "circulation" or "rotation" in a fluid and is defined as $\nabla \times \mathbf{u}$ where $\mathbf{u}$ is the fluid velocity. The six different instants are chosen during one cardiac cycle and are marked with the circles '○' in the right panel of Fig. 8. The first instant is chosen when the artery has the smallest diameter.

In case of the normal artery, see Fig. 9, the blood flows down with small vortex sheddings in the systolic phase (second and third columns) and then as a result of vortex multiplication, large symmetric vortices are generated from the original vortex in the diastolic phase (fourth to sixth columns) after 1.30 s (this is when the heart starts to relax after contraction or after the artery maximizes its diameter). The blood pressure during systole is approximately linear along the arterial wall from the inlet to the outlet (see the 2nd and 3rd pressure contours) and the pressure during diastole shows the large vortical pressure difference. There is not much difference in the pressure distribution during deceleration, which is also true for the dilated and constricted arteries, see Figs. 10 and 11. However, the pressure difference between the top and the bottom during systole is higher in the constrictive artery than in the normal artery or in the bulging artery (see 3rd pressure contours in Figs. 9–11). Note that the blood pressure at each time does not change much, spatially, inside the artery. The change of the pressure becomes more distinct in the temporal direction; see the difference of colors in the panels of the pressure contours.

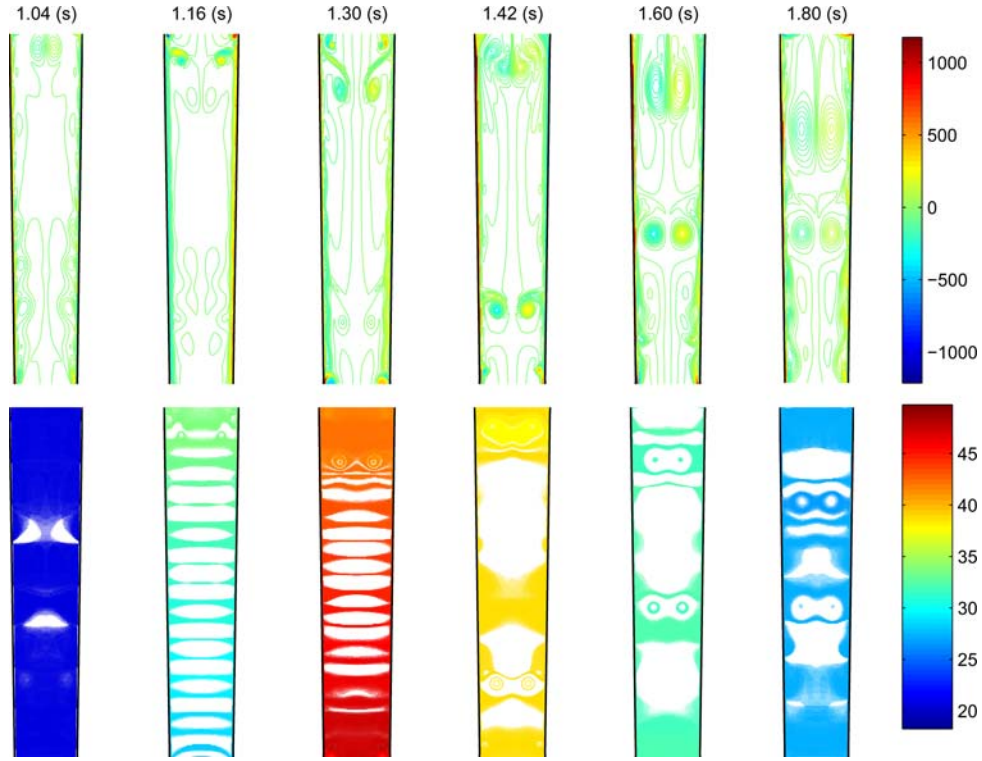

FIGURE 9. Normal artery. Vorticity contours (top) and pressure contours (bottom) are shown at some fixed times. The chosen times over one cardiac cycle are marked with circles '○' in the right panel of Fig. 8. The unit of vorticity is in s^{-1} and that of pressure is in mmHg.

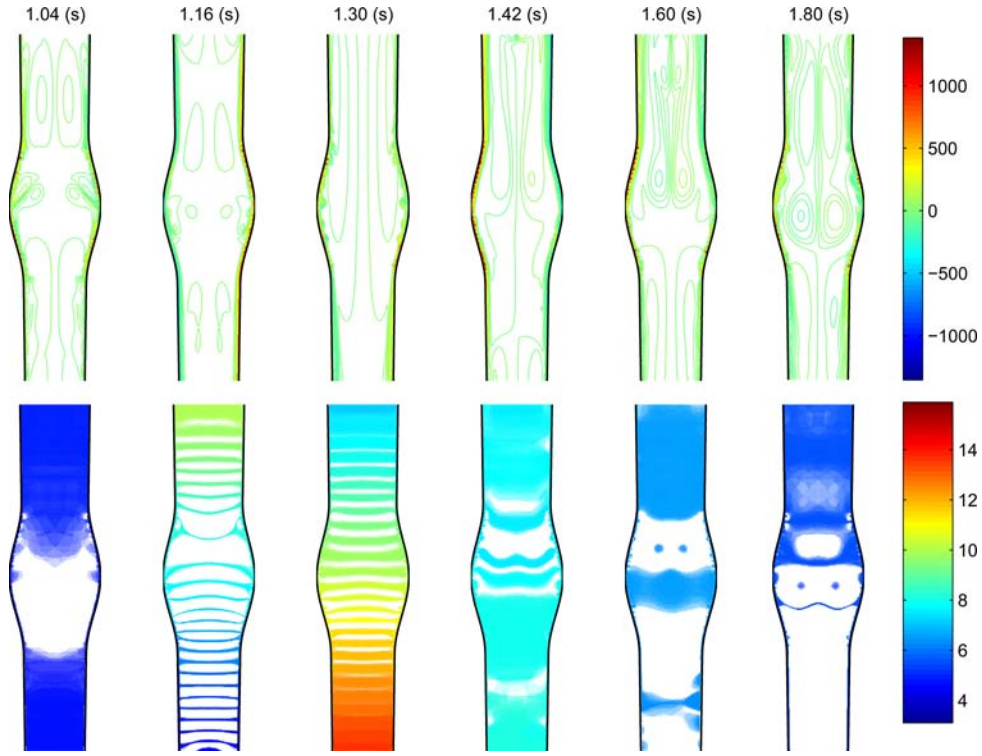

FIGURE 10. Symmetric bulge in the artery. The top panels show the vorticity contours and the bottom panels show the pressure contours at different times over one cardiac cycle. The unit of vorticity is in s^{-1} and that of pressure is in mmHg.

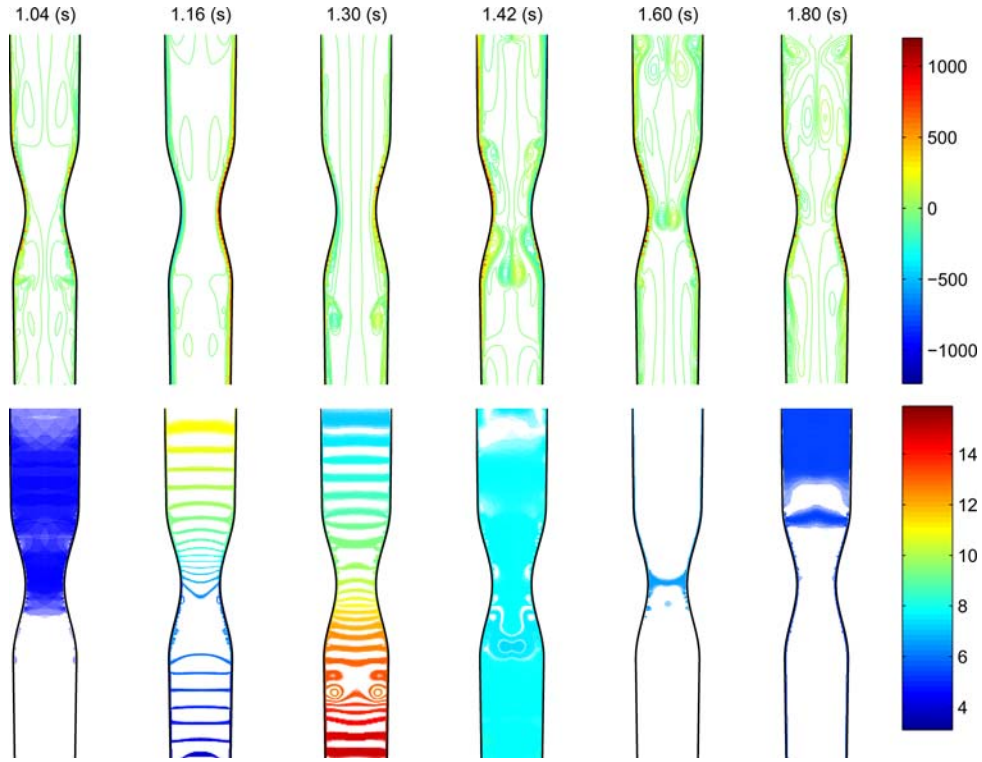

FIGURE 11. Symmetric constriction in the artery. The top panels show the vorticity contours and the bottom panels show the pressure contours at different times over one cardiac cycle. The unit of vorticity is in s^{-1} and that of pressure is in mmHg.

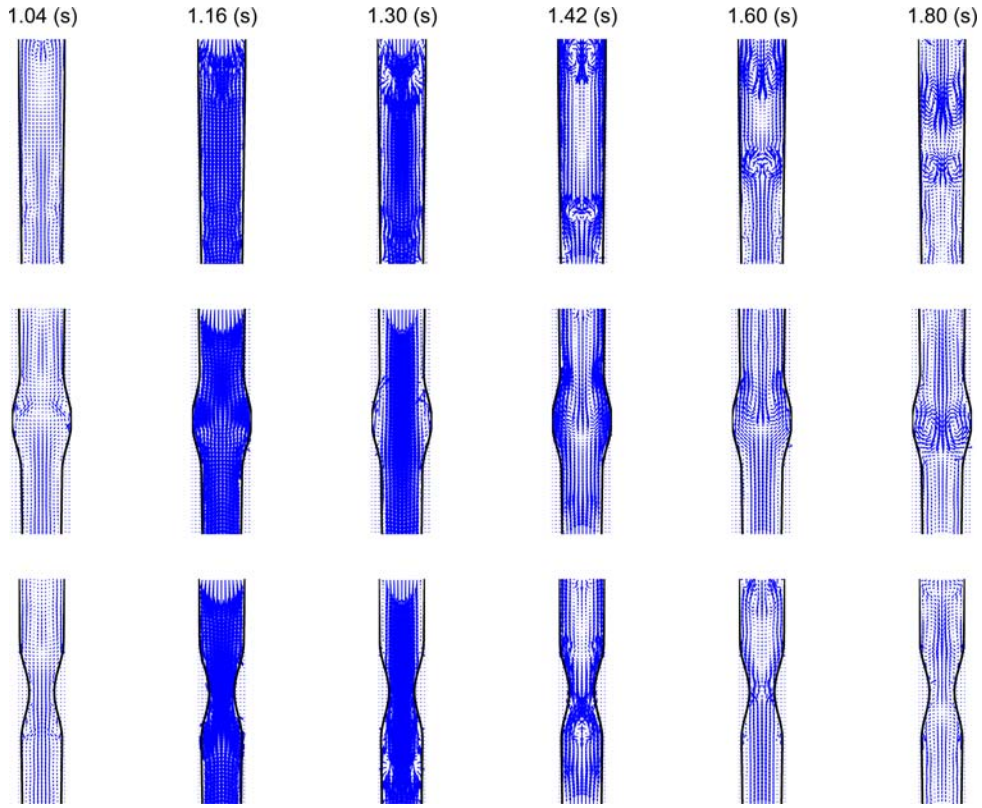

FIGURE 12. Velocity vector fields over one cardiac cycle in different shapes of blood vessel: (top) normal artery, (middle) aneurysmal artery, and (bottom) stenotic artery.

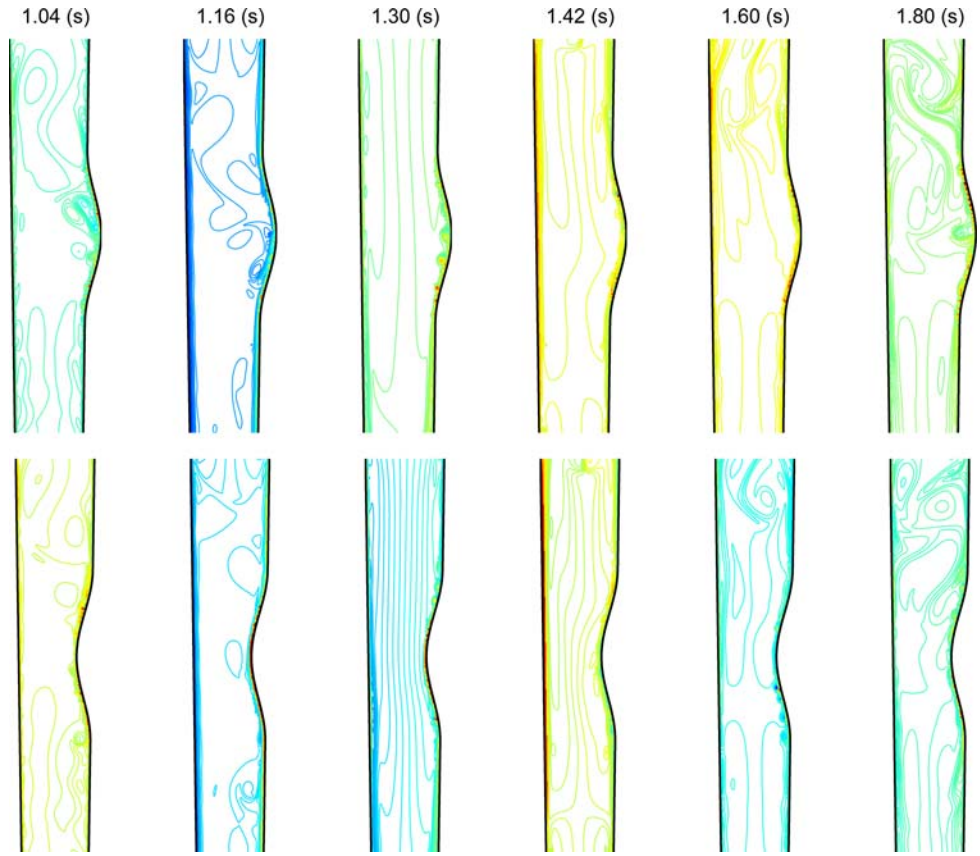

FIGURE 13. Asymmetric arteries. The vorticity contours at different times over one cardiac cycle are shown for the asymmetric bulge (top) and the asymmetric constriction (bottom) in the arteries. The unit of vorticity is in s^{-1} and that of pressure is in mmHg.

In the dilated and constrictive arteries, the vortex structure and the pressure difference are similar to those of the normal artery, see Figs. 10 and 11. The vortices during systole are small, and the vortices during diastole are large and clear. The pressure inside the artery during systole is distributed almost linearly along the vessel wall both in the constrictive and dilated arteries. In the stenotic artery the flow accelerates through stenosis and recirculates at the downstream.

Figure 12 shows velocity vector fields over one cardiac cycle. Three different configurations of blood vessel are considered. First row corresponds to the velocity vector field in the normal artery, middle row corresponds to the velocity field in the aneurysmal artery, and bottom row corresponds to the velocity field in the stenotic artery. As expected, blood flows rapidly from the top to the bottom in systole in all cases. During diastole we can see the backflow as observed in the experimental data.

Figure 13 shows vorticity contours in the asymmetric dilated artery (top) and in the asymmetric constrictive artery (bottom). The figure shows the asymmetric vortex structure unlike the symmetric abnormal cases.

DISCUSSION

The two-dimensional mathematical model developed in this work describes the interaction between blood flow and the arterial wall. It is important to consider a coupled system of fluid–structure interaction, because the pulsatile flow will affect the aortic wall movement, and this movement in turn will influence the flow pattern. We used the IB method to describe the motion of the arterial wall and analyze the flow pattern inside the vessel, and the mathematical model was validated by comparison with Womersley flow which is the well-known solutions of Navier–Stokes equations in a pipe when the pressure gradient is known.

In the computer simulations we prescribed the upstream velocity using the MR data and the downstream velocity using the transmural pressure reproduced from the literature. The method we use computes only the pressure gradient, not the pressure level. Thus, the blood pressure based on the experimental data has to be prescribed either at the inlet or at the outlet in order to obtain the pressure distribution inside the vessel. In this way, we can simulate the

interaction between blood and a vessel wall using the realistic blood velocity and pressure value inside a large artery.

As mentioned in section "Two-dimensional Vessel Model", we have assumed that the same fluid fills the computational domain, i.e., both inside and outside the vessel. This assumption might result in a limitation for some applications such as a blood vessel in a bone, in the lung, or near the skin. However, this assumption is reasonable for the problems of blood flow in major arteries because the density of the tissues outside a large blood vessel is about the same as that of blood. Thus, our mathematical model includes the inertial and viscous loads provided by the external tissues by having same densities inside and outside of the blood vessel.

There may also be some ways to deal with forces acting on the wall due to the external tissues or organs. First, one can replace those forces by prescribing pressure condition along the wall, as is commonly done.[9,16,40,43] Second, one can place elastic fibers or layers outside the vessel so that forces by the external medium can be represented by the elastic forces of the fibers.

In our computations, hysteresis is captured in the relation between the blood pressure and the diameter of the artery. We can only observe the hysteresis behavior when the viscoelastic property of the arterial wall is taken into consideration in the model, as reported in literature. The mass of the vessel wall and the viscosity of the fluid do not effect this hysteresis.

We considered five different initial configurations: a straight but tapered artery, a symmetric dilated artery, an asymmetric dilated artery, a symmetric constrictive artery, and an asymmetric constrictive artery, and compare the flow patterns inside the vessel for these configurations. Generally large vortices are generated during deceleration after systole, and these vortices move down slowly with blood and stay longer in diastolic artery.

The goal of this research is to apply a computational model to real patients who have aneurysms or stenosis. The precise cause of aneurysms and stenosis is still unknown; however, the common belief is that they result from the interplay between the dynamics of blood flow on the arterial wall and biological processes in the wall. Therefore, computational simulations of blood flow dynamics coupled with the arterial wall may provide physical insight into the hemodynamics in both normal and abnormal arteries.

Generally, the IB method is easy and simple to implement and the computation time does not take long, since the FFT is used as a fluid solver for a system of discretized Navier–Stokes equations. Another advantage of the IB method is that one can create any shape or structure using elastic fibers in the three-dimensional space. These fibers could be made rigid or flexible. It is known that the arterial wall consists of fibers such as elastin fibers, collagen fibers (much stiffer than elastin), and smooth muscle fibers. These fibers run in different directions, for example, some fibers are arranged in circumferential or helical directions. Thus, it is necessary to extend our 2D model to a three-dimensional model of blood flow in a compliant vessel in order to describe the full dynamics of the arterial wall. In addition, the wall thickness can also be represented by several layers and each layer is composed of elastic fibers. The IB method enables us to construct an arterial wall based on the actual structure and to interpret properly the material properties of the wall.

ACKNOWLEDGMENTS

We would like to thank both Tam Tran and Ghalib Bello for their technical assistance. We are also indebted to Charles Peskin for the useful discussion. This research was supported by National Science Foundation upon Agreement No. 0112050.

REFERENCES

[1]Armentano, R. L., J. G. Barra, J. Levenson, A. Simon, and R. H. Pichel. Arterial wall mechanics in conscious dogs: assessment of viscous, inertial, and elastic moduli to characterize aortic wall behavior. *Circ. Res.* 76:468–478, 1995.

[2]Armentano, R. L., J. L. Megnien, A. Simon, F. Bellenfant, J. G. Barra, and J. Levenson. Effects of hypertension on viscoelasticity of carotid and femoral arteries in humans. *Hypertension* 26:48–54, 1995.

[3]Arthurs, K. M., L. C. Moore, C. S. Peskin, E. B. Pitman, and H. E. Layton. Modeling arteriolar flow and mass transport using the immersed boundary method. *J. Comput. Phys.* 147:402–440, 1998.

[4]Bauer, R. D., R. Busse, A. Shabert, Y. Summa, and E. Wetterer. Separate determination of the pulsatile elastic and viscous forces developed in the arterial wall in vivo. *Pflugers Arch.* 380:221–226, 1979.

[5]Berger, S. A., and L. Jou. Flows in stenotic vessels. *Annu. Rev. Fluid Mech.* 32:347–382, 2000.

[6]Beyer, R. P. A computational model of the cochlea using the immersed boundary method. *J. Comput. Phys.* 98:145–162, 1992.

[7]Boal, D. Mechanics of the Cell. Cambridge University Press, 2002, pp. 31–32.

[8]Boudoulas, H., P. K. Toutouzas, and C. F. Wooley. Functional Abnormalities of the Aorta. Futura Publishing Company, 1996.

[9]Canic, S., C. J. Hartley, D. Rosenstrauch, J. Tambaca, G. Guidoboni, and A. Mikelic. Blood flow in compliant arteries: an effective viscoelastic reduced model, numerics and experimental validation. *Ann. Biomed. Eng.* 34(4):575–592, 2006.

[10]Dillon, R., L. Fauci, and D. Gaver, III. A microscale model of bacterial swimming, chemotaxis and substrate transport. *J. Theor. Biol.* 177:325–340, 1995.
[11]Dillon, R., L. Fauci, and C. Omoto. Mathematical modeling of axoneme mechanics and fluid dynamics in ciliary and sperm motility. *Dyn. Contin. Discret. Impul. Syst.* 10(5):745–757, 2003.
[12]Duraiswamy, N. Stented artery flow patterns and their effects on the artery wall. *Annu. Rev. Fluid Mech.* 39:357–382, 2007.
[13]Fauci, L., and C. S. Peskin. A computational model of aquatic animal locomotion. *J. Comput. Phys.* 77:85–108, 1988.
[14]Fogelson, A. L. A mathematical model and numerical method for studying platelet adhesion and aggregation during blood clotting. *J. Comput. Phys.* 56:111–134, 1984.
[15]Fogelson, A. L., and C. S. Peskin. A fast numerical method for solving the three-dimensional Stoke's equations in the presence of suspended particles. *J. Comput. Phys.* 79:50–69, 1988.
[16]Formaggia, L., D. Lamponi, and A. Quarteroni. One-dimensional models for blood flow in arteries. *J. Eng. Math.* 47:251–276, 2003.
[17]Ganten, M., *et al.* Quantification of aortic distensibility in abnormal aortic aneurysm using ECG-gated multi-detector computed tomography. *Eur. Radiol.* 18:966–973, 2008.
[18]Giannattasio, C., M. Failla, and G. Emanuelli. Local effects of atherosclerotic plaque on arterial distensibility. *Hypertension* 38(5):1177–1180, 2001.
[19]Givelberg, E. Modeling Elastic Shells Immersed in Fluid. Ph.D.Thesis, Mathematics, New York University, 1997.
[20]Hung, T. K., and M. C. Tsai. Pulsatile blood flows in stenotic artery. *J. Eng. Mech.* 122(9):890–896, 1996.
[21]Jung, E., and C. S. Peskin. Two-dimensional simulations of valveless pumping using the immersed boundary method. *SIAM J. Sci. Comput.* 23:19–45, 2001.
[22]Kim, Y. The Penalty Immersed Boundary Method and its Application to Aerodynamics. Ph.D.Thesis, Mathematics, New York University, 2003. UMI ProQuest Digital Dissertations. Publication Number AAT 3105887.
[23]Kim, Y., and C. S. Peskin. 2-D parachute simulation by the Immersed Boundary Method. *SIAM J. Sci. Comput.* 28(6):2294–2312, 2006.
[24]Kim, Y., and C. S. Peskin. Penalty immersed boundary method for an elastic boundary with mass. *Phys. Fluids* 19(5):053103–053103-18, 2007.
[25]Kleinstreuer, C., L. Li, and M. A. Farber. Fluid-structure interaction analyses of stented abdominal aortic aneurysms. *Annu. Rev. Biomed. Eng.* 9:169–204, 2007.
[26]Kovacs, S. J., D. M. McQueen, and C. S. Peskin. Modeling cardiac fluid dynamics and diastolic function. *Phil. Trans. R. Soc. Lond. A* 359:1299–1314, 2001.
[27]Lasheras, J. C. The biomechanics of arterial aneurysms. *Annu. Rev. Fluid. Mech.* 39:293–319, 2007.
[28]Lehmann, E. D., and R. G. Gosling. Measuring aortic distensibility. *Lancet* 338:1075, 1991.
[29]Lim, S., and C. S. Peskin. Simulations of Whirling Instability by the immersed boundary method. *SIAM J. Sci. Comput.* 25:2066–2083, 2004.
[30]Malek, A. M., S. L. Alper, and S. Izumo. Hemodynamics shear stress and its role in atherosclerosis. *JAMA* 282(21):2035–2042, 1999.
[31]Megnien, J. L., A. Simon, F. Bellenfant, J. G. Barra, and J. Levenson. Effects of hypertension on viscoelasticity of carotid and femoral arteries in humans. *Hypertension* 26:48–54, 1995.
[32]Nichols, W., and M. O'Rourke. McDonald's Blood Flow in Arteries. London: Edward Arnold Ltd., 2005.
[33]Pedersen, E. M., H. Sung, A. C. Burlson, and A. P. Yoganathan. Two-dimensional velocity measurements in a pulsatile flow model of the normal abdominal aorta simulating different hemodynamic conditions. *J. Biomech.* 26(10):1237–1247, 1993.
[34]Peskin, C. S. Numerical analysis of blood flow in the heart. *J. Comput. Phys.* 25:220–252, 1977.
[35]Peskin, C. S., and D. M. McQueen. Three dimensional computational method for flow in the heart: immersed elastic fibers in a viscous incompressible fluid. *J. Comput. Phys.* 81:372–405, 1989.
[36]Peskin, C. S., and D. M. McQueen. A general method for the computer simulation of biological systems interacting with fluids. *Symp. Soc. Exp. Biol.* 49:265–276, 1995.
[37]Peskin, C. S., and D. M. McQueen. Fluid dynamics of the heart and its valves. Case Studies in Mathematical Modeling: Ecology, Physiology, and Cell Biology. Englewood Cliffs, NJ: Prentice Hall, 1996, pp. 309–337.
[38]Peskin, C. S., and D. M. McQueen. Heart simulation by an immersed boundary method with formal second-order accuracy and reduced numerical viscosity. In: Mechanics for a New Millennium, Proceedings of the International Conference on Theoretical and Applied Mechanics (ICTAM) 2000, edited by H. Aref and J. W. Phillips. Kluwer Academic Publishers, 2001.
[39]Quarteroni, A., M. Tuveri, and A. Veneziani. Computational vascular fluid dynamics: problems, models, and methods. *Comput. Visual. Sci.* 2:163–197, 2000.
[40]Sherwin, S. J., L. Formaggia, J. Peiró, and V. Franke. Computational modelling of 1D blood flow with variable mechanical properties and its application to the simulation of wave propagation in the human arterial system. *Int. J. Num. Method Fluid* 43(6–7):673–700, 2003.
[41]Stary, H. C. Atlas of Atherosclerosis: Progression and Regression. 2nd ed. London: Parthenon Publishing, 2003.
[42]Stefanadis, C., C. Vlachopoulos, P. Karayannocos, *et al.* Effect of vasa vasorum flow on structure and function of the aorta in experimental animals. *Circulation* 91:2669–2678, 1995.
[43]Tang, D., and J. Yang. A free moving boundary model and boundary iteration method for unsteady viscous flow in stenotic elastic tubes. *SIAM J. Sci. Comput.* 21(4):1370–1386, 2000.
[44]Wilson, K. A., A. J. Lee, P. R. Hoskins, *et al.* The relationship between aortic wall distensibility and rupture of infrarenal abdominal aortic aneurysm. *J. Vasc. Surg.* 37(1):112–117, 2003.
[45]Wolinsky, H., and S. Glagov. A lamellar unit of aortic medial structure and function in mammals. *Circ. Res.* 20:99–111, 1967.
[46]Womersley, J. R. Method for the calculation of velocity, rate of flow and viscous drag in arteries when the pressure gradient is known. *J. Physiol.* 127:553–563, 1955.
[47]Zhu, L., and C. S. Peskin. Simulation of a flapping flexible filament in a flowing soap film by the immersed boundary method. *J. Comput. Phys.* 179:452–468, 2002.